Case Studies in Thermal Engineering 63 (2024) 105322

Contents lists available at ScienceDirect

Case Studies in Thermal Engineering

journal homepage: www.elsevier.com/locate/csite

Thermal analysis of nonlinear mixed convection effects within wavy enclosure

Arooj Tanveer [a,*], Sami-ul-Haq [a], Muhammad Bilal Ashraf [a], JongSuk Ro [b,c]

[a] *Department of Mathematics, COMSATS University Islamabad (CUI), 455000, Park Road, Tarlai Kalan, Islamabad, Pakistan*
[b] *School of Electrical and Electronics Engineering, Chung Ang University, Dongjak-gu, Seoul, 06974, Republic of Korea*
[c] *Department of Intelligent Energy and Industry, Chung-Ang University, Dongjak-gu, Seoul, 06974, Republic of Korea*

A R T I C L E I N F O

Keywords:
Hybrid nanofluids
MHD
Nonlinear mixed convection
Wavy cavity
Nusselt number
ANN

A B S T R A C T

The analysis in this study focuses on the transfer of heat within a wavy cavity in the presence of nonlinear mixed convection and MHD. We conduct the investigation under conditions where the upper wall of the cavity remains cold, the lower wall receives heat, and the left and right wavy walls remain adiabatic. Using the PDE solver in COMSOL, the non-dimensional system is simplified, employing the finite element method. The study aims to explore the impact of parameters such as nanoparticle concentration, Hartmann number, Reynolds number, Richardson number, and nonlinear mixed convection parameters on fluid flow and heat transfer. An artificial neural network has been employed to examine the behaviour of the Nusselt number within a cavity. The isotherms reveal that the temperature is higher near the lower wall for all parameters due to the heated source. Analysis of the streamline plots indicates that heat increases as it moves towards the upper wall, influenced by the Hartman number and volume fraction parameter. The use of ANN in the study forecasts the accuracy, smoothness, and convergence of the data through plots of mean squared error (MSE), error histogram, regression analysis, and transition state plot. The authors believe that using artificial neural networks to explore the heat transfer rate under the assumptions of MHD and nonlinear mixed convection is a novel approach that has not been previously investigated. Additionally, researchers can utilise ANN concepts to predict intricate cavity formations through multiphysics. This approach will require less human effort and computing time to analyse the heat response of any dataset.

1. Introduction

A highly advanced class of computer models known as artificial neural networks (ANNs) draws inspiration from the intricate biological neural network architecture present in the human brain. Their inherent ability to solve difficult problems through parallel processing and data-driven learning accounts for their broad use in a variety of industries. As a result, several professions have advanced significantly, showcasing their ability to understand and solve difficult problems. In the study of artificial intelligence and machine learning, artificial neural networks are an effective tool. An artificial neural network (ANN) is a network of interconnected nodes or neurones that is highly effective at solving complex problems, enabling high-level abstraction, and seeing minute patterns in large datasets. Communication is made possible by weighted connections between neurones at various levels, which aid in the network's processing of incoming data and conversion of it into meaningful and contextually relevant output. Notably, the design of the ANN is naturally flexible, allowing for the investigation of various network configurations, such as feed-forward, recurrent,

* Corresponding author.
E-mail address: uroojtanveer496@gmail.com (A. Tanveer).

https://doi.org/10.1016/j.csite.2024.105322
Received 26 July 2024; Received in revised form 22 September 2024; Accepted 21 October 2024
Available online 1 November 2024

and convolutional architectures, all of which are customised to target particular applications and problem domains. Artificial neural networks (ANNs) have shown great promise in fluid mechanics for handling complicated problems such as modelling complex fluid flow phenomena, predicting unsteady flow behaviour, characterising turbulent dynamics, and optimising flow management strategies. In order to investigate the natural convection of alumina/H2O nanofluids (NFs) moving inside a cavity, Alqaed et al. [1] used the volume control technique in conjunction with the SIMPLE algorithm.Mandal et al. [2] investigated the thermal behaviour of an M-shaped cavity filled with hybrid nanofluids using the Levenberg Marquardt method. Rana et al. [3] investigated spontaneous convection in an inclined hollow filled with a magnetohydrodynamic (MHD) hybrid nanofluid, Cu-Al2O3. The water contains suspended Cu-Al2O3 nanoparticles. This study uses an artificial neural network approach to investigate the Nusselt number.

Due to their intentional blending of several types of nanoparticles or useful additives, hybrid nanofluids are a step above traditional nanofluids. The goal of this strategic integration is to improve thermal transport qualities in a way that works in concert, giving rise to enhanced and customised heat transfer capabilities. By utilising several types of nanoparticles or additives, hybrid nanofluids can simultaneously optimise many thermal parameters, increasing heat transfer efficiency and, in some situations, providing multifunctional performance. The creation of hybrid nanofluids using analytical means entails a thorough investigation of the connections among different nanoparticle interactions, surface functionalisation, and colloidal stability. Extensive studies of this kind are necessary to optimise the arrangement in order to maximise the synergistic effects of individual components and provide notable improvements in the heat transport characteristics. Because of this, the field of hybrid nanofluids is a promising one for tackling difficult thermal problems in a variety of engineering applications; however, for its successful application and revolutionary effect, it will require interdisciplinary research efforts involving fluid mechanics, materials science, and heat transfer. The emerging field of hybrid nanofluids shows great potential for solving complex thermal problems that are common in modern engineering applications. However, to fully use their potential and turn these cutting-edge materials into workable solutions for the next generation of thermal management, a coordinated interdisciplinary approach combining the principles of fluid mechanics, heat transfer, and materials science is required. Understanding the complexities that dictate the behaviour of hybrid nanofluids and utilising their potential to efficiently tackle complex heat transfer problems requires an exhaustive and meticulous investigation across these several fields. The revolutionary potential of hybrid nanofluids can only be fully realised through such coordinated research efforts, opening the door to cutting-edge and effective thermal management solutions with far-reaching consequences. In a work by Abderrehmanne et al. [4], the buoyancy-driven flow of a nanofluid inside a cavity under the influence of a magnetic field was analysed using the Galerkin Finite Element Method (FEM). The goal of Anirban et al. [5] was to examine the thermal behaviour of magneto-mixed convection in a wavy cavity that was filled with a nanofluid made up of suspended Cu-Al2O hybrid nanoparticles. They came to the conclusion that improved thermal performance was a result of the larger volume fraction. Hamid and Alireza [6] investigated the heat transfer that occurs naturally convecting from an Al2O3-Cu nanoparticle-dispersed hybrid nanofluid inside an open wavy cavity. The heat transfer phenomenon was studied and simulated using the lattice Boltzmann method scheme. The study concentrated on the system's reactions to a uniform magnetic field. The conjugate free convection flow, heat transmission, and entropy production properties of hybrid nanofluids comprising suspended copper-alumina nanoparticles in water were investigated by Alsabery et al. [7]. These nanofluids were examined in a chamber that was only partially split. Because of the increased thermal conductivity that resulted from increasing the volumetric flow rate and volume percentage of nanoparticles, the researchers found that heat transfer was improved. The use of hybrid nanofluids in various enclosures is demonstrated in the literature [8–15].

A branch of physics known as magneto-hydrodynamics (MHD) is an interdisciplinary field that studies electrically conducting fluids under magnetic fields. Principles from plasma physics, electromagnetism, and fluid dynamics are all interwoven in this intricate field. The importance of MHD may be found in many different natural and artificial systems, including space plasmas, fusion reactors, astrophysical events, and geophysical manifestations like the dynamics of the magnetosphere and the earth's magnetic field. When magnetic fields are introduced, they have a significant impact on the development of turbulence and instabilities in electrically conducting fluids. These effects display complex behaviours that resist simple explanations and therefore require the critical application of MHD as a framework to explore their complex relationships. As a result, this information has practical use in engineering fields since it makes it possible to control and reduce turbulence in real-world applications like propulsion systems and MHD power generation. MHD has been used by researchers in conjunction with other phenomena such as joule heating, various media, etc. For example, Mansour and Bakir [16] examined the effects of MHD over hybrid nanofluids within the porous double lid-driven cavity using the finite difference approach. They concluded that the magnetic field strengthens the thermal equilibrium condition by balancing forced and spontaneous convection. The focus of Rahmoune and Bogol's [17] study is on how the dynamic properties of an Al2O3-water nanofluid contained in a cavity and magnetohydrodynamic (MHD) natural convection phenomena interact and impact each other. Through the interaction of these phenomena, complex fluid flow and heat transfer behaviour are seen, and their analysis aims to provide deeper insights into these behaviours. The flow behaviour of a Fe3O4/MWCNT-water mixture was examined by Jiang et al. [18] in a 3D cubic enclosure with a porous edium. The research conducted by Hussein et al. [19] uses numerical methods to study the properties of stable magnetohydrodynamic (MHD) mixed convection in an inclined two-dimensional (2D) cavity with vertical walls that are wavy.

This study explores the complex relationships between heat transport and fluid dynamics in a wavy cavity heated by a source of light. We utilise the most advanced combination of magnetohydrodynamics (MHD) and hybrid nanofluids (Cu-Tio2/H2O) to tackle these intricacies. We employ Comsol Multiphysics and the Levenberg–Marquardt technique of Artificial Neural Networks (ANN) to investigate the Nusselt number in detail with the goal of revealing the enhanced heat transfer capabilities present in these new nanofluid configurations. The utilisation of an artificial neural network for the thermal analysis within a wavy cavity has not been accomplished so far in the literature, making it a novel approach to studying the thermal changes within the cavity. Numerous disciplines, including energy systems, electronics cooling, medicinal research, metallurgical operations, and environmental studies,

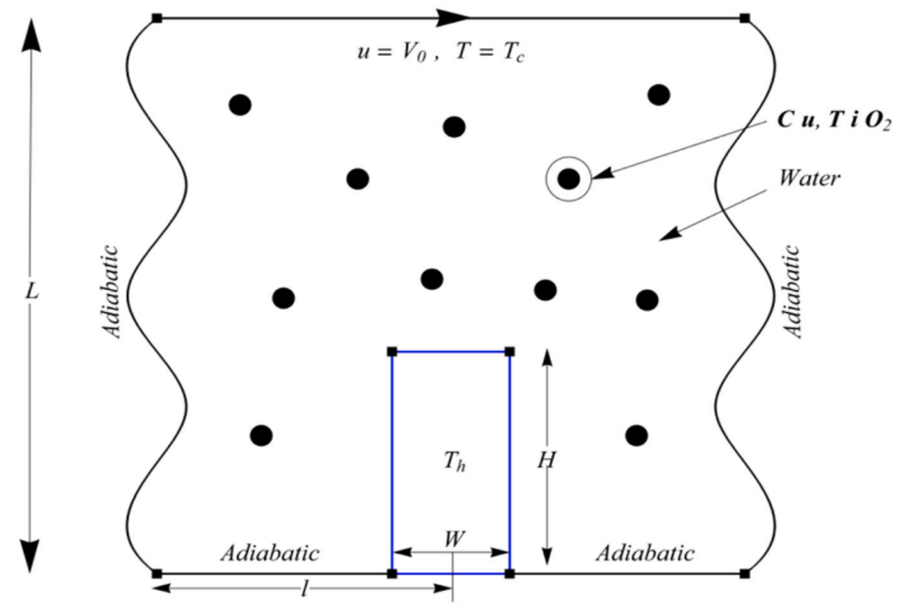

Fig. 1. Geometry of the problem.

employ wavy cavities in viscous fluids with mixed convection and MHD. While the use of magnetohydrodynamics (MHD) enables precise manipulation of fluid behaviour, the special shape of wavy cavities improves fluid mixing, heat transport, and flow control. To optimise processes in engineering and industrial applications, it is important to comprehend these connections.

2. Mathematical modelling

This study investigates the incompressible two-dimensional flow characteristics of a hybrid nanofluid in a unit-length (L) wavy square cavity. The cavity has fixed and adiabatic sides, and the cold top wall is moving in the direction of positive x. A heated rectangular source, measuring 0.4 inches in height and 0.2 inches in width, is resting on the base of the chamber. Nonlinear mixed convection effects and a magnetic field are also included in the analysis as important variables. As seen in Fig. 1, the application of the magnetic field is perpendicular to the horizontal walls. The hybrid nanofluid in the square cavity is made up of copper (Cu) and titanium dioxide (TiO_2) nanoparticles mixed with water, which serves as the base fluid.

The governing system of equations are:

$$\frac{\partial u}{\partial x} + \frac{\partial v}{\partial y} = 0 \tag{1}$$

$$u\frac{\partial u}{\partial x} + v\frac{\partial u}{\partial y} = -\frac{1}{\rho_{\text{hnf}}}\frac{\partial p}{\partial x} + \frac{\mu_{\text{hnf}}}{\rho_{\text{hnf}}}\left(\frac{\partial^2 u}{\partial x^2} + \frac{\partial^2 u}{\partial y^2}\right) \tag{2}$$

$$\begin{aligned} u\frac{\partial v}{\partial x} + v\frac{\partial v}{\partial y} = &-\frac{1}{\rho_{\text{hnf}}}\frac{\partial p}{\partial y} + \frac{\mu_{\text{hnf}}}{\rho_{\text{hnf}}}\left(\frac{\partial^2 v}{\partial x^2} + \frac{\partial^2 v}{\partial y^2}\right) - \frac{\sigma_{\text{hnf}}}{\rho_{\text{hnf}}}B_0^2 v \\ &+ g\left(\beta_{1_{\text{hnf}}}(T - T_c) + \beta_{2_{\text{hnf}}}(T - T_c)^2\right) \end{aligned} \tag{3}$$

$$(\rho C_p)_{\text{hnf}}\left(u\frac{\partial T}{\partial x} + v\frac{\partial T}{\partial y}\right) = k_{\text{hnf}}\left(\frac{\partial^2 T}{\partial x^2} + \frac{\partial^2 T}{\partial y^2}\right) \tag{4}$$

With boundary conditions:

At the upper wall of cavity

$$u = V_0, v = 0, T = T_c, y = L, \quad 0 \le x \le L \tag{5}$$

Left adiabatic wavy wall of cavity

$$u = 0 = v, \frac{\partial T}{\partial x} = 0, \quad L - A(1 - cos(2Nx)), \quad 0 \le y \le L \tag{6}$$

Right adiabatic wavy wall of cavity

$$u = 0 = v, \frac{\partial T}{\partial x} = 0, \quad A(1 - cos(2Nx)), \quad 0 \le y \le L \tag{7}$$

At the lower adiabatic wall of cavity

$$u = 0, v = 0, \frac{\partial T}{\partial x} = 0, y = 0, \quad 0 \le x \le (l - W/2) \ \ and \ \ l + W/2 \le x \le L \tag{8}$$

At the upper side of heated source

$$u = 0 = v, T = T_h, y = H, l - W/2 \le x \le l + W/2 \tag{9}$$

At the left side of heated source

$$u = 0 = v, T = T_h, x = l - W/2, \quad 0 \le y \le H \tag{10}$$

At the right side of heated source

$$u = 0 = v, T = T_h, x = l + W/2, 0 \le y \le H \tag{11}$$

here, Eq. (3) has MHD and nonlinear terms on the right side of equation. Eq. (5) shows that upper wall is moving with velocity V_0. The different quantities like σ_{hnf}, ρ_{hnf}, B, p, g, T_h, T_c, $(C_p)_{hnf}$, k_{hnf}, and $(\beta_1)_{hnf}$ represent the electric conductivity of nanofluid, nanofluid density, external applied magnetic field, pressure, gravitational acceleration, hot wall temperature, cold wall temperature, specific heat capacity of nanofluids, thermal conductivity of nanofluids, and thermal expansion coefficient of nanofluids, respectively. The following dimensionless variables are used in Eqs. (1)–(11):

$$X = \frac{x}{L}, \quad Y = \frac{y}{L}, \quad U = \frac{u}{v_0}, \ P = \frac{p}{\rho_{hnf} v_0^2}, \ \theta = \frac{T - T_c}{T_h - T_c} \tag{12}$$

The obtained dimensionless system is:

$$U\frac{\partial U}{\partial X} + V\frac{\partial V}{\partial Y} = 0 \tag{13}$$

$$U\frac{\partial U}{\partial X} + V\frac{\partial U}{\partial Y} = -\frac{\partial P}{\partial X} + \frac{1}{F_1 F_2}\frac{1}{Re}\left(\frac{\partial^2 U}{\partial X^2} + \frac{\partial^2 U}{\partial Y^2}\right) \tag{14}$$

$$\begin{aligned} U\frac{\partial U}{\partial X} + V\frac{\partial U}{\partial Y} = &-\frac{\partial P}{\partial Y} + \frac{1}{F_1 F_2}\frac{1}{Re}\left(\frac{\partial^2 U}{\partial X^2} + \frac{\partial^2 U}{\partial Y^2}\right) \\ &- \frac{F_6}{F_1}\frac{M^2}{Re}V + \frac{F_3}{F_1}Ri(\theta + \alpha\theta^2). \end{aligned} \tag{15}$$

$$U\frac{\partial \theta}{\partial X} + V\frac{\partial \theta}{\partial Y} = \frac{F_5}{F_4}\frac{1}{RePr}\left(\frac{\partial^2 \theta}{\partial X^2} + \frac{\partial^2 \theta}{\partial Y^2}\right) \tag{16}$$

The dimensionless boundary conditions of the problem are:
At the upper wall of cavity

$$U = 1, V = 0, T = 0, Y = L, 0 \le X \le L \tag{17}$$

Left adiabatic wavy wall of cavity

$$U = 0 = V, \frac{\partial \theta}{\partial X} = 0, L - A(1 - cos(2N\pi X)), \quad 0 \le Y \le L \tag{18}$$

Right adiabatic wavy wall of cavity

$$U = 0 = V, \frac{\partial \theta}{\partial X} = 0, A(1 - cos(2N\pi X)), \quad 0 \le Y \le L \tag{19}$$

At the lower adiabatic wall of cavity

$$U = 0 = V, \frac{\partial \theta}{\partial Y} = 0, Y = 0, 0 \le X \le l - W/2 \ \ and \ \ l + W/2 \le X \le L \tag{20}$$

At the upper side of heated source

$$U = 0 = V, \theta = 1, Y = H, \quad l - W/2 \le X \le l + W/2 \tag{21}$$

At the left side of heated source

$$U = 0 = V, \theta = 1, X = l - W/2, \quad 0 \le Y \le H \tag{22}$$

At the right side of heated source

$$U = 0 = V, \theta = 1, X = l + W/2, \quad 0 \le Y \le H \tag{23}$$

Here, the physical parameters are Prandtl number(ratio of momentum to thermal diffusivity), Reynolds number (ratio of inertial to viscous forces), Richardon number (ratio of potential to kinetic energy density), Grashof parameter (), hartman number. F_1 to F_6

are symbols used to represent long expressions involved in equations due to hybrid nanofluids thermophysical parameters . They are given in Eq. (24):

$$
\begin{aligned}
&\mathrm{Pr}=\frac{\mu_f (C_p)_f}{k_f}, \quad \mathrm{Re}=\frac{V_0 L}{\nu_f}, \quad \mathrm{Ri}=\frac{\mathrm{Gr}}{\mathrm{Re}^2},\\
&\mathrm{Gr}=\frac{g(\beta_1)_f (T_h-T_c)L^3}{\nu_f^2}, \quad M=B_0 L\sqrt{\frac{\sigma_f}{\mu_f}}, \quad \alpha=\frac{(\beta_2)_f (T_h-T_c)}{(\beta_1)_f},\\
&F_1=\frac{\phi_1\rho_{S1}}{\rho_f}+\frac{\phi_2\rho_{S2}}{\rho_f}+(1-\phi_{hnf}), \quad F_2=(1-\phi_{hnf})^{2.5}\\
&F_3=\frac{\phi_1(\rho\beta)_{S1}}{(\rho\beta)_f}+\frac{\phi_2(\rho\beta)_{S2}}{(\rho\beta)_f}+(1-\phi_{hnf}), \quad F_4=\frac{\phi_1(\rho C_p)_{S1}}{(\rho C_p)_f}+\frac{\phi_2(\rho C_p)_{S2}}{(\rho C_p)_f}+(1-\phi_{hnf})\\
&F_5=\frac{\left(\frac{\phi_1 k_1+\phi_2 k_2}{\phi_{hnf}}+2(\phi_1 k_1+\phi_2 k_2)+2(1-\phi_{hnf})k_f\right)}{\left(\frac{\phi_1 k_1+\phi_2 k_2}{\phi_{hnf}}-(\phi_1 k_1+\phi_2 k_2)+(2+\phi_{hnf})k_f\right)},\\
&F_6=\left(1+\frac{3\left(\left(\phi_1\sigma_{s1}+\phi_2\sigma_{s2}\right)/\sigma_f-\phi_{hnf}\right)}{\left(\left(\phi_1\sigma_{s1}+\phi_2\sigma_{s2}\right)/\sigma_f+2\right)-\left(\left(\phi_1\sigma_{s1}+\phi_2\sigma_{s2}\right)/\sigma_f-\phi_{hnf}\right)}\right)
\end{aligned}
\tag{24}
$$

The Nusselt number is used to evaluate the heat transfer rate at the heated or cold walls. The dimensionless local nusselt numbers of the sides of heated source are given as:

$$\mathrm{Nu}_l=-F_5\left(\frac{\partial\theta}{\partial X}\right)_{(l-\frac{W}{2})}$$

$$\mathrm{Nu}_r=-F_5\left(\frac{\partial\theta}{\partial X}\right)_{(l+\frac{W}{2})}$$

$$\mathrm{Nu}_u=-F_5\left(\frac{\partial\theta}{\partial Y}\right)_{(Y=H)}$$

The total local Nusselt number is defined as:

$$Nu=Nu_l+Nu_r+Nu_u$$

The total average Nusselt number of the sides of heated source is.

$$\mathrm{Nu}_{\mathrm{av}}=\frac{1}{3}\left(\int_{(l-\frac{W}{2})}^{(l+\frac{W}{2})}\mathrm{Nu}_u\,dX+\int_0^H \mathrm{Nu}_l\,dY+\int_0^H \mathrm{Nu}_r\,dY\right)$$

3. Research methodology

In this section, the method for studying heat transfer in a wave-shaped cavity, which incorporates nonlinear mixed convection effects and magnetohydrodynamics (MHD), is described. The governing system of equations is solved using the PDE solver finite element method in COMSOL. It took one minute and 39 s to complete the Comsol analysis. In the first phase, the solution domain is discretised into a finite number of meshes, or networks of irregular triangle elements. Then, we developed the finite element equations using the six-node triangular elements. Following that, we convert the nonlinear PDEs into an integral equation structure using the Galerkin weighted residual approach. Gauss' quadrature technique is used to integrate and solve each of those equations. By applying the boundary conditions, we alter the nonlinear algebraic equations. Datasets generated by COMSOL, which vary various parameters for the average Nusselt number, are divided into three groups: training, validation, and testing. We train an ANN using the Levenberg–Marquardt approach using these sets. To begin, we accumulate a total of five hundred distinct outcomes for the Nusselt numbers. Sparing 70 percent for training, 15 percent for validation, and 15 percent for testing is the current data allocation dilemma. During training, the network takes in inputs and target datasets and changes its structure according to the mistakes it makes. Training can be stopped when validation determines that the diffusion of information inside a network has reached a certain threshold. Since testing has no effect on training, it offers a valid pre- and post-training evaluation of the network's performance. An example of a multi-layer back-propagated neural network is shown in Fig. 3. Ten neurones and four inputs make up the hidden layer used in the study. Following that, we evaluate the ANN model's efficacy by checking its training status, mean square error, error histogram, regression analysis, and overall performance. For the hybrid nanofluid flow problem under study, this proves that the ANN-based approach is accurate and reliable in predicting the average Nusselt number.

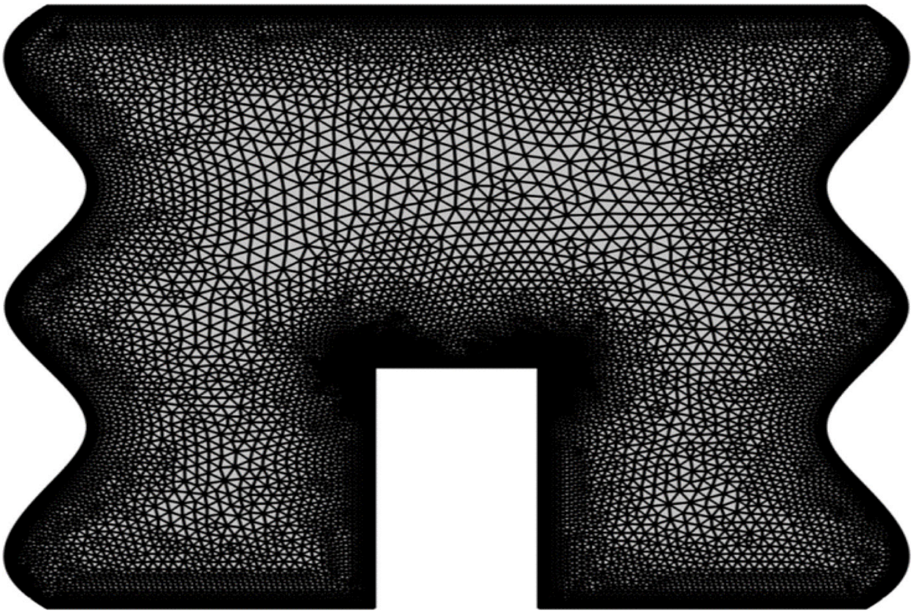

Fig. 2. Triangular Mesh.

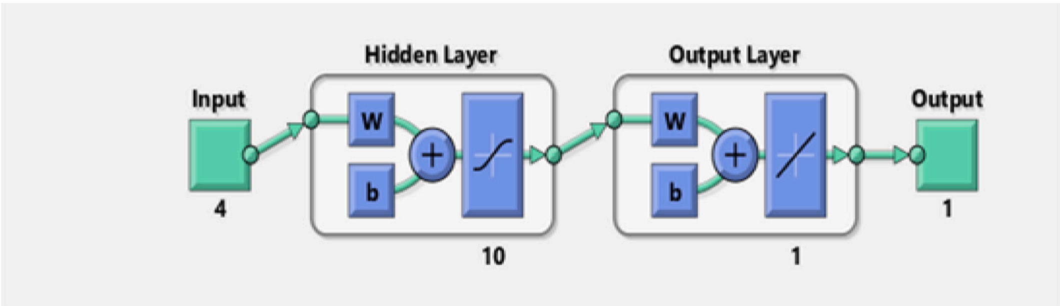

Fig. 3. Architecture of the neural network.

4. Model validation

The current study is validated with Kefayti and Huigol [20] work for the present model within a wavy cavity. All of the findings, as shown in Fig. 4(a–b), are in accord with one another, with a negligible rate of errors. As demonstrated in Table 1, the Nu_{avg} values for grids 8 and 9 are approximately the same. Hence, in order to keep computational costs down, this study uses the average Nusselt number from the extra-fine mesh size simulations, which include 21136 mesh elements and 748 boundary elements with $Nu_{avg} = 15.599$.

5. Results and discussion

5.1. Effect of Hartman number (M)

In Fig. 5(a–f), the magnetic field causes the production of distinctive flow patterns around an enclosed rectangular heat source. These flow patterns' strength and direction are influenced by the magnetic parameter. The changing behaviour of streamlines shows that velocity is gradually decreasing due to the increasing impact of magnetic fields. The isotherms show that temperature is high near a heated source but gradually declines due to a strong magnetic field. The magnetic field's presence assists heat transfer because it improves fluid mixing and modifies flow patterns. As a result, the temperature inside the cavity reduces due to more effective heat dispersion from the rectangular heated source.

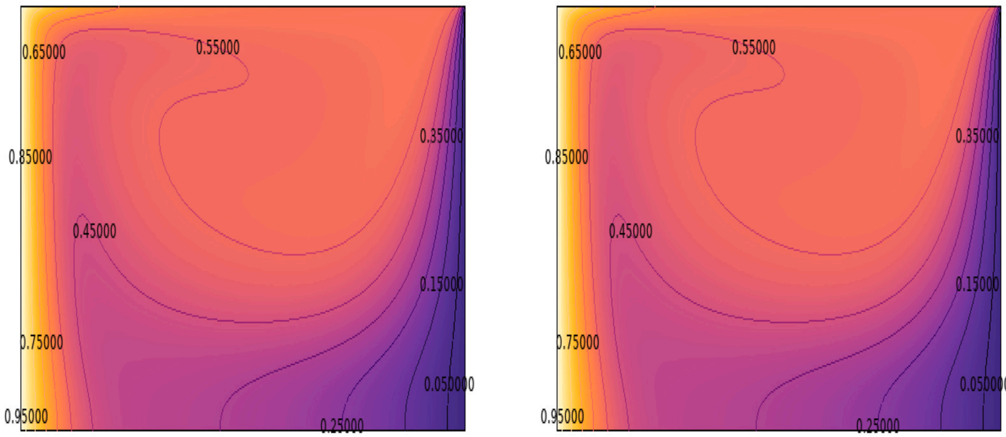

(a) Reference work [20]. (b) Present model.

Fig. 4. Validation test for isotherm Re = 500.

Table 1
Grid sensitivity check for Nu_{avg} at Re = 500.

Mesh size	Mesh elements	Boundary elements	Nu_{avg}	Error
Extremely coarse	251	41	10.8973	
Extra coarse	420	60	11.063	0.06%
Coarser	665	77	11.9455	0.03%
Coarse	1223	113	12.5324	0.05%
Normal	1873	145	12.8363	0.03%
Fine	3154	180	13.461	0.02%
Finer	8334	386	14.707	0.08%
Extra Fine	21 136	748	15.599	0.07%
Extremely Fine	32 892	748	15.601	0%

5.2. Effect of volume fraction parameter of nanofluids

Fig. 6(a–f) demonstrates the impact of concentration of hybrid nanoparticles on the streamlines for $0.2 < \phi < 0.6$. For higher concentrations of nanoparticles, the vortex near the heated source starts diminishing. The convective heat transfer behaviour of the flow is affected by nanoparticles. The temperature distribution is uniform along isothermal contours, which improves the efficiency of heat transfer from the heat source to the ambient environment. Compared to the base fluid, nanoparticles often have substantially higher thermal conductivities. The overall thermal conductivity of the nanofluid increases along with the volume fraction of nanoparticles.

The Nusselt number rises when the volume proportion of scattered particles or phases in a fluid increases in Fig. 7. The main source of this improvement is the fluid's increased thermal conductivity, which is brought on by the presence of high-conductivity nanoparticles. The overall thermal conductivity of the nanofluid increases as the volume percentage of nanoparticles does, resulting in more effective heat transfer and a larger Nusselt number.

5.3. Effect of Richardson parameter

Fig. 8(a–f) depicts the impact of the Richardson parameter on streamlines and isotherms for $Ri > 1/4$. Vortices are moving towards the right wall, and new eddies are formed near the heated source. However, the isotherms are showing that the area

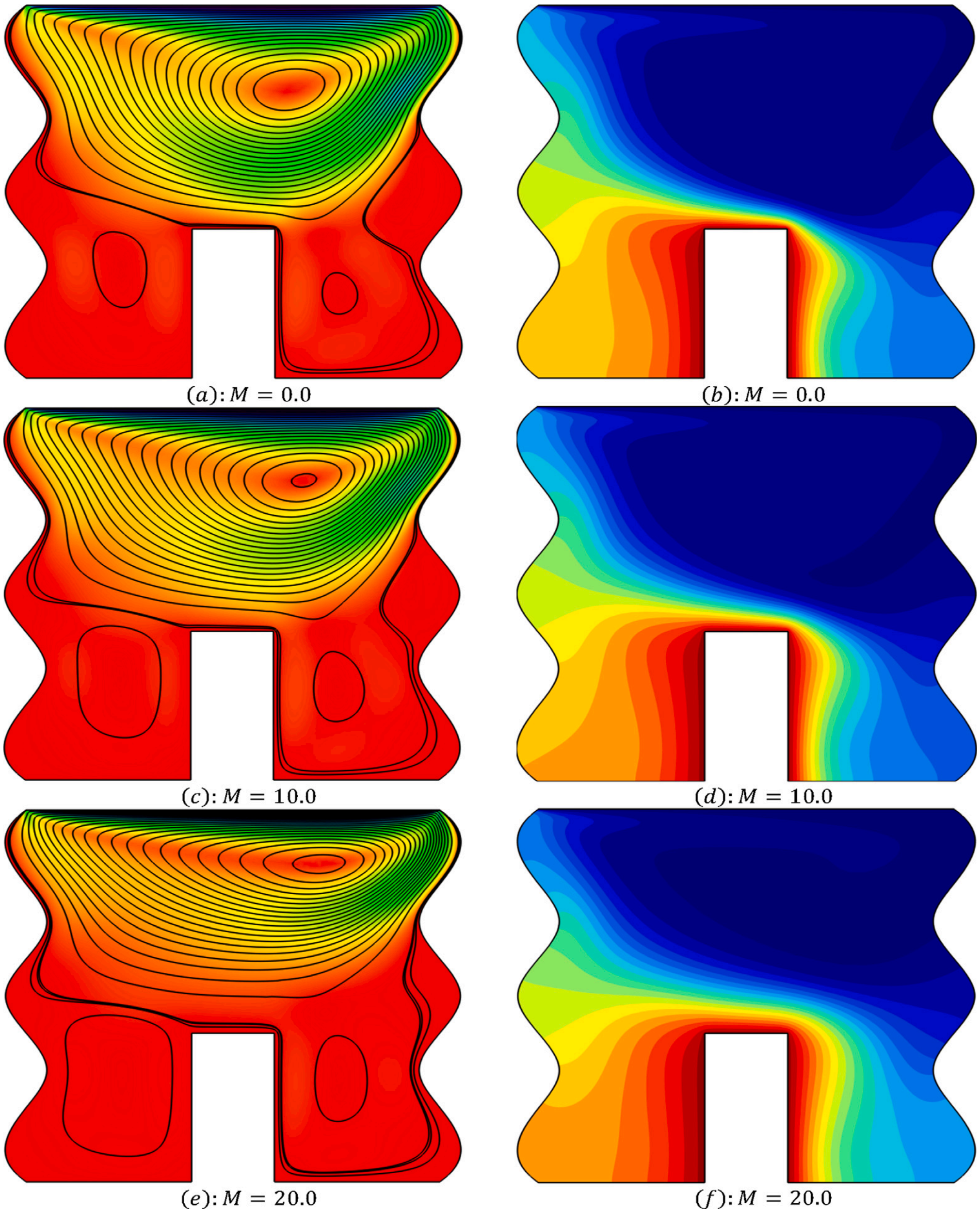

Fig. 5. Impact of magnetic parameter on streamlines and isotherms.

around the rectangular heated source is becoming colder with rising values of Ri. The Nusselt number shows a change that led to its increase due to the dominancy of buoyancy forces in Fig. 9.

5.4. Effect of Reynolds parameter

Fig. 10(a–f) defines the change in streamlines and isotherms due to the higher Reynolds number. Higher Reynolds numbers cause the flow in a wavy cavity to become more turbulent, which causes the geometry to change and the inertial forces to increase, causing more eddies to form. It is since, when compared to viscous forces, inertial forces take precedence, which intensifies turbulence. Higher Reynolds numbers and the phenomenon of accelerated heat transfer are the main causes of the temperature drop along isotherms in turbulent flow. Because of the turbulent eddies, there is an increase in momentum transfer between fluid layers in turbulent flow. A more even distribution of temperatures is achieved because of the more effective transfer of heat from hotter to

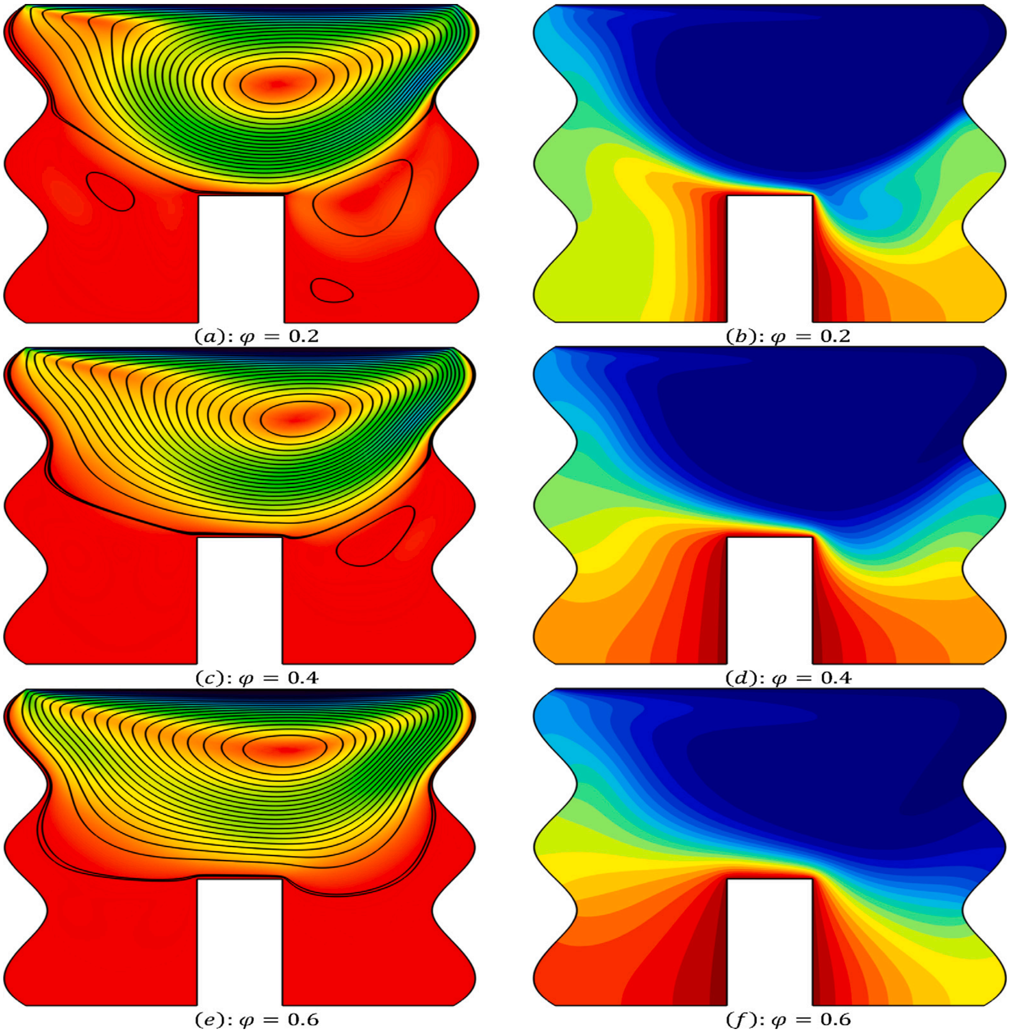

Fig. 6. Impact of volume fraction coefficient on streamlines and isotherms.

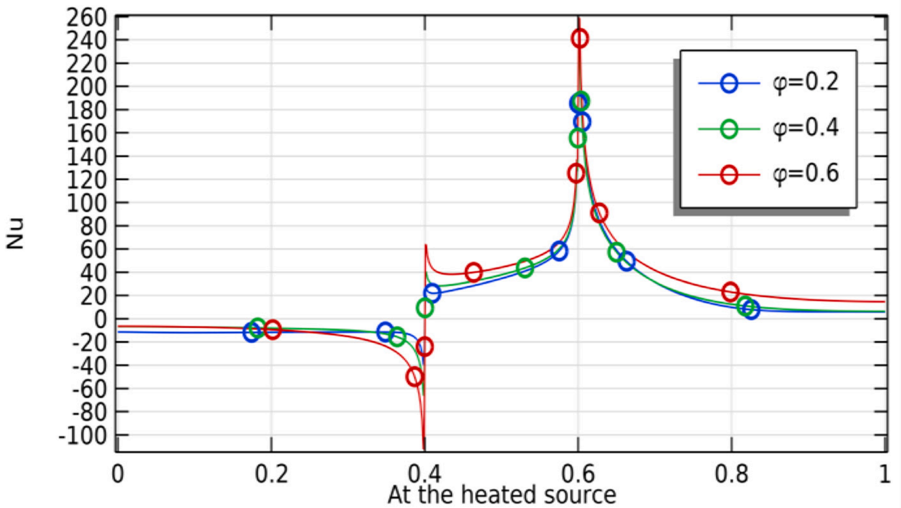

Fig. 7. Impact of volume fraction coefficient on Nusselt number.

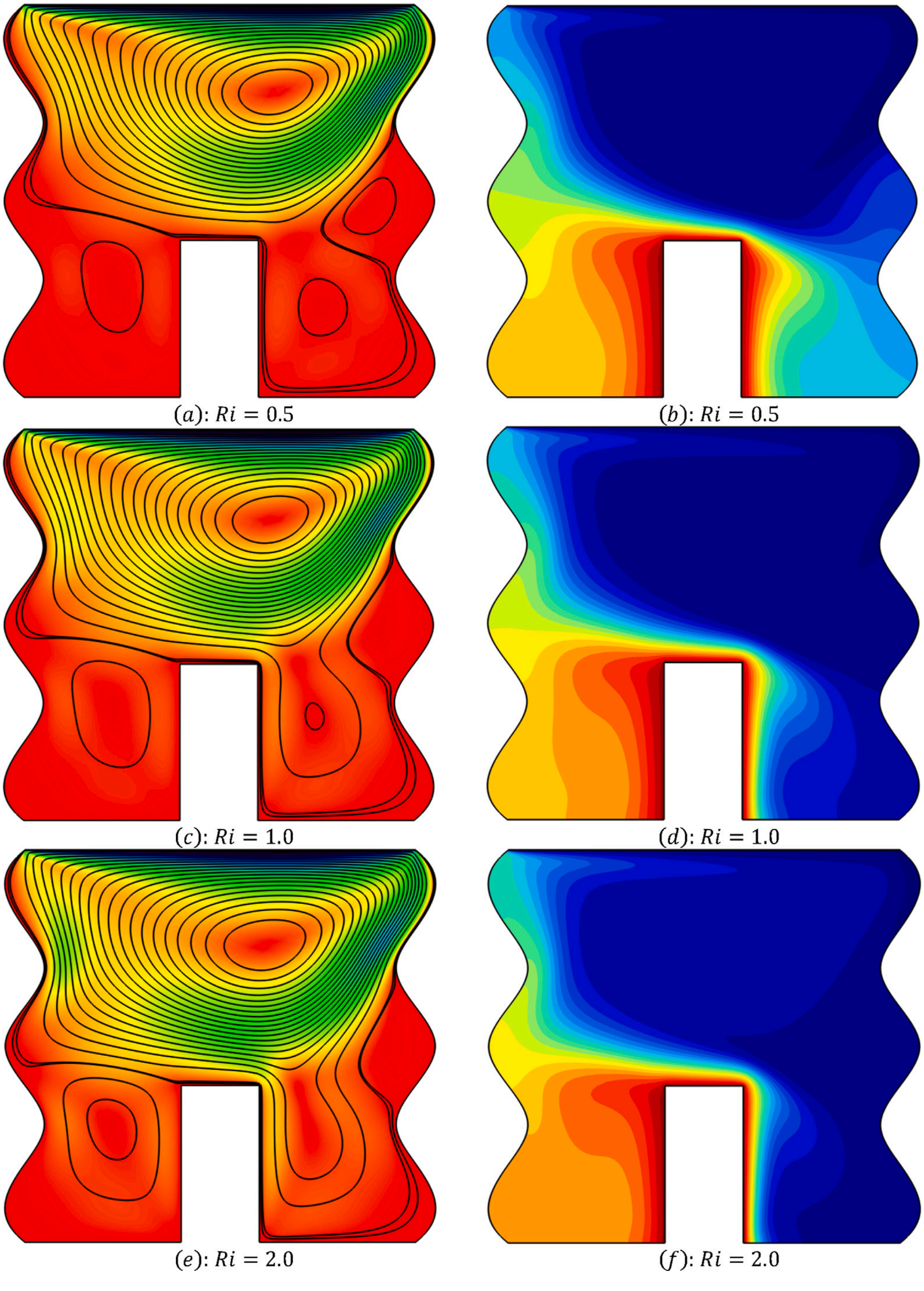

Fig. 8. Impact of Richardson parameter on streamlines and isotherms.

colder areas. Fig. 11 shows that the flow is more abrupt when Re> 100, which improves heat transmission and raises the Nusselt number.

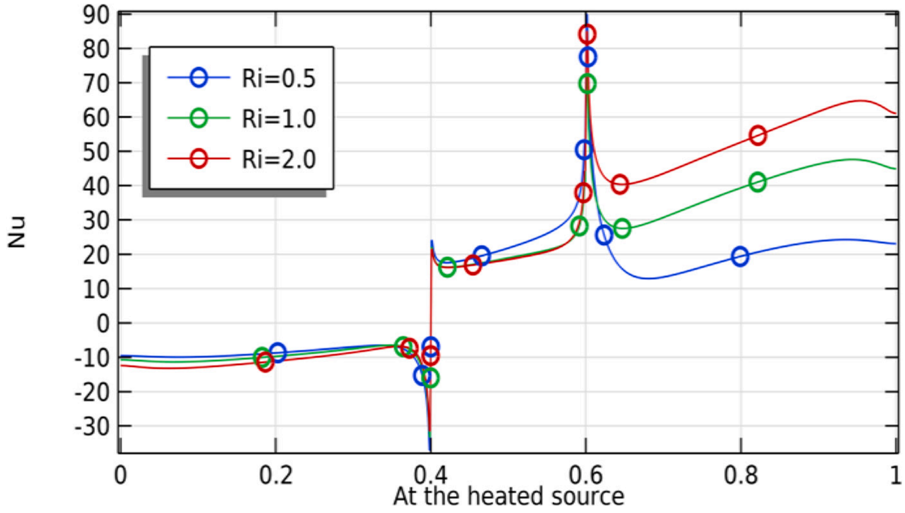

Fig. 9. Impact of Richardson number on Nusselt number.

Table 2
Thermophysical properties correlation.

Physical properties	Hybrid nanofluid
Viscosity (μ)	$\mu_{\mathrm{hnf}} = \frac{\mu_f}{(1-\phi_{\mathrm{hnf}})^{2.5}}$
Density (ρ)	$\rho_{\mathrm{hnf}} = \phi_1 \rho_{\mathrm{S1}} + \phi_2 \rho_{\mathrm{S2}} + \rho_f (1 - \phi_{\mathrm{hnf}})$
Heat Capacity (ρC_p)	$(\rho C_p)_{\mathrm{hnf}} = (1 - \phi_{\mathrm{hnf}})(\rho C_p)_f + \phi_1 (\rho C_p)_{\mathrm{S1}} + \phi_2 (\rho C_p)_{\mathrm{S2}}$
Thermal conductivity (k)	$k_{\mathrm{hnf}} = \left[\frac{\left(\frac{\phi_1 k_1 + \phi_2 k_2}{\phi_{\mathrm{hnf}}} + 2(\phi_1 k_1 + \phi_2 k_2) + 2(1-\phi_{\mathrm{hnf}}) k_f \right)}{\left(\frac{\phi_1 k_1 + \phi_2 k_2}{\phi_{\mathrm{hnf}}} - (\phi_1 k_1 + \phi_2 k_2) + (2+\phi_{\mathrm{hnf}}) k_f \right)} \right] \times k_f$
Electrical conductivity (σ)	$\sigma_{\mathrm{hnf}} = \sigma_f \left(1 + \frac{3\left(\frac{\phi_1 \sigma_{\mathrm{S1}} + \phi_2 \sigma_{\mathrm{S2}}}{\sigma_f} - \phi_{\mathrm{hnf}} \right)}{\left(\frac{\phi_1 \sigma_{\mathrm{S1}} + \phi_2 \sigma_{\mathrm{S2}}}{\sigma_f} + 2 \right) - \left(\frac{\phi_1 \sigma_{\mathrm{S1}} + \phi_2 \sigma_{\mathrm{S2}}}{\sigma_f} - \phi_{\mathrm{hnf}} \right)} \right. \Big/ \left(\left(\frac{\phi_1 \sigma_{\mathrm{S1}} + \phi_2 \sigma_{\mathrm{S2}}}{\sigma_f} + 2 \right) - \left(\frac{\phi_1 \sigma_{\mathrm{S1}} + \phi_2 \sigma_{\mathrm{S2}}}{\sigma_f} - \phi_{\mathrm{hnf}} \right) \right) \Bigg)$

Table 3
Thermo-physical properties for hybrid nanofluids.

Physical Properties	H_2O	CuO	TiO_2
C_p (J/(kg K))	4197	385	686.2
$\rho(\mathrm{kg/m^3})$	997.1	8933	4250
k(W/mK)	0.613	401	48.953
$\sigma(\frac{s}{m})$	0.05	$5.96e^7$	$6.28e^{-5}$
$\beta_1(\frac{1}{K})$	$21e^{-5}$	$1.67e^{-5}$	$0.9e^{-5}$

5.5. Effect of nonlinear mixed convection parameter α

Fig. 12(a–f) describes the changing behaviour of streamlines and isotherms for higher values of α. Buoyancy forces play a more significant role in controlling the fluid flow with higher values of the nonlinear mixed convection parameter. Buoyancy-driven flows are naturally unstable and prone to the formation of vortices. Thus, more vortices are produced for $\alpha > 0$ in Fig. 12. In the case of isotherms, the increase in α leads to no temperature near the right wall of the heated source, and the overall wavy cavity becomes colder. The interaction of buoyant forces and external forcing in this convection causes changes in the flow pattern. The behaviour of the fluid is increasingly affected by flows generated by buoyancy as the nonlinear mixed convection parameter is raised. As a result, the fluid experiences a redistribution of heat, with cooler areas flowing nearer the hot surface and lowering the surface temperature. In Fig. 13, the stronger external forcing caused by the increased nonlinear mixed convection parameter causes the fluid to move and turbulence to increase. Because of the improved heat transmission from the heated surface to the surrounding fluid made possible by the increased fluid motion, the Nusselt number is larger.

For a wavy cavity filled with hybrid nanofluids and an enclosed square heat source, this study assesses the effect of several factors such as the Hartmann number, volume fraction, Richardson, and Reynolds number. Details on the CFD-obtained mesh points are shown in Fig. 2. The data reveals that there are 23428 points in the mesh. Table 2 provides the formulas for viscosity, density, thermal and electrical conductivity, heat capacity, and thermal expansion, as type-II hybrid nanofluids are utilised for the analysis.

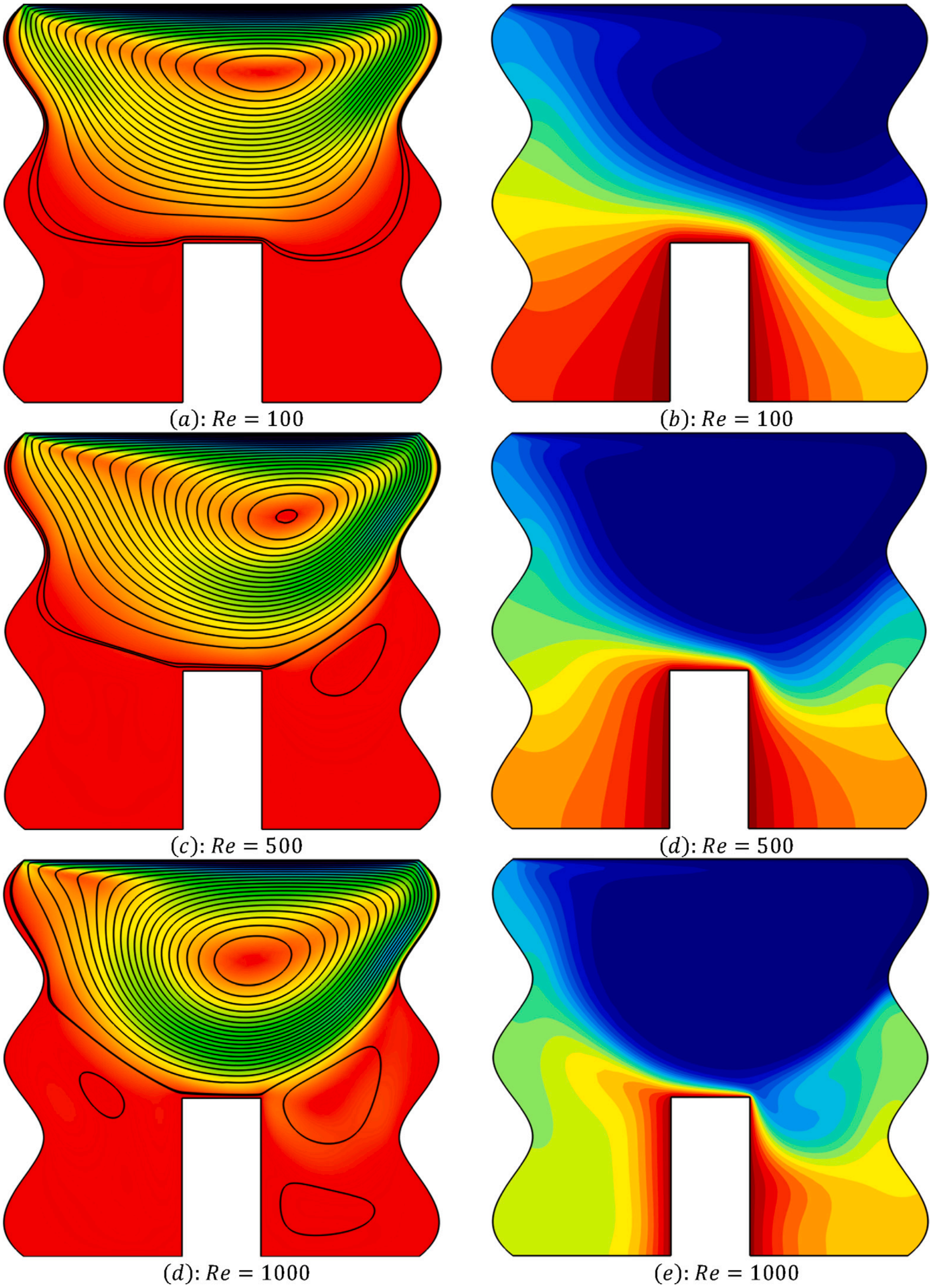

Fig. 10. Impact of Reynolds parameter on streamlines and isotherms.

Table 3 displays the thermophysical characteristics of the base fluid (H2O) and the solid (CuO/TiO2). A look at the MSE, regression values, and LMS performance analysis in Tables 4 and 5 reveals some interesting insights for various stages. For training data, the MSE is 1.39568 e^{-7}, for validation data, it is 9.39281 e^{-6}, and for testing data, it is 1.03700 e^{-1}, as shown in Table 3. The correctness and stability of the optimisation process are demonstrated by these values. The network's total performance analysis is shown in Table 2. After 1000 epochs, it reached a minimal gradient of 0.000184 in 33 s. The system's parameters mentioned above, as shown in Fig. 3, come in a range of values across four input layers. There are ten neurones in the hidden layer that activate the Tan sigmoid

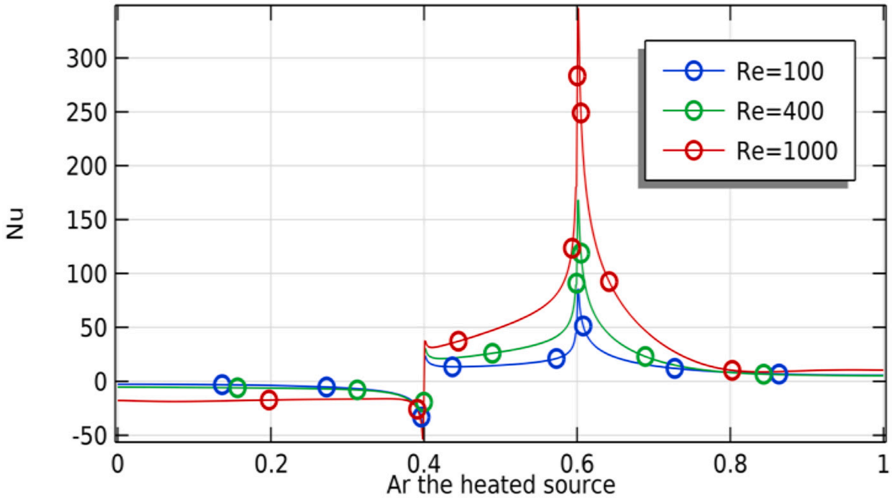

Fig. 11. Impact of Reynolds number on Nusselt number.

Table 4
Values of MSE and R through LMS.

ANN model	MSE	R
Training	$1.39568e^{-7}$	$9.99999e^{-1}$
Validation	$9.39281e^{-6}$	$9.99989e^{-1}$
Testing	$1.03700e^{-1}$	$8.27895e^{-1}$

Table 5
Performance analysis through LMS.

Epoch	Time	Performance	Gradient	Mu	Validation checks
1000	0:00:33	$1.40e^{-7}$	0.000184	$1e^{-7}$	6

function, which is used to assess the data. The analysis of the Nusselt number is conducted using the back-propagated method in artificial neural networking. The nusselt number of the model is assessed in relation to the fluctuation of several factors.

Mean Square Error (MSE) is a popular statistic utilised in artificial neural networks (ANN) to assess the efficacy of a regression model. As a whole, it is a measure of how far off the actual values are from the expected values. Fig. 14 indicates that the best validation performance, with an MSE of $9.3928e^{-6}$, is achieved at epoch 1000. The mean squared error (MSE) of network prediction produced during training, and then applying optimisation methods like gradient descent to reduce the error. By doing so, the parameters (weights and biases) of the network are fine-tuned to enhance its performance. A lower MSE value is obtained in the MSE graph, increasing the stability and dependability of the solution.

Fig. 15 demonstrates the transition state plot obtained from LMS consisting of gradient, Mu, and validation fail data information. The training process dynamics, such as the optimisation algorithm's convergence behaviour, the impact of learning rate on convergence speed, and the presence of overfitting, can be better understood by examining the transition state map, which illustrates these elements. The gradient value of 1.8378e−6 is obtained at epoch 1000, and it is observed that gradient values tend to decrease as the analysis progresses. Here we can see the error function's steepest decline, along with its direction and amplitude. Put another way, it indicates the direction where the greatest rise in error is likely to occur. Thus, a falling gradient indicates that the optimisation technique (for example, gradient descent) is coming closer and closer to achieving the lowest possible value of the error function. Mu is a hyperparameter referred to as learning rate. If the learning rate is too low during training, the optimisation process will take longer to converge. As Fig. 15 shows, Mu is $1e^{-}07$ after 1000 epochs. It implies that this small learning rate took a lot of runs before it found a good enough solution. The validation check is zero, which means there is no overfitting of the data. Higher training and testing efficiency lead to better alignment between the conclusions concerning the minimal Mu and gradient, as indicated by the graph.

Another approach used to evaluate training performance is the inspection of error histograms, which show the errors achieved during training. Targeted and ANN-predicted values are used to obtain the error histograms. For each of the twenty vertical bins, they are displayed. Fig. 16 illustrates that the given model is producing low-variance, accurate predictions with no bias; this is an ideal result for machine learning tasks since there is just one bin with a zero line near −0.04404 in the error histogram. To sum up, the results are very accurate, with only a little margin of error between the projected and actual outcomes.

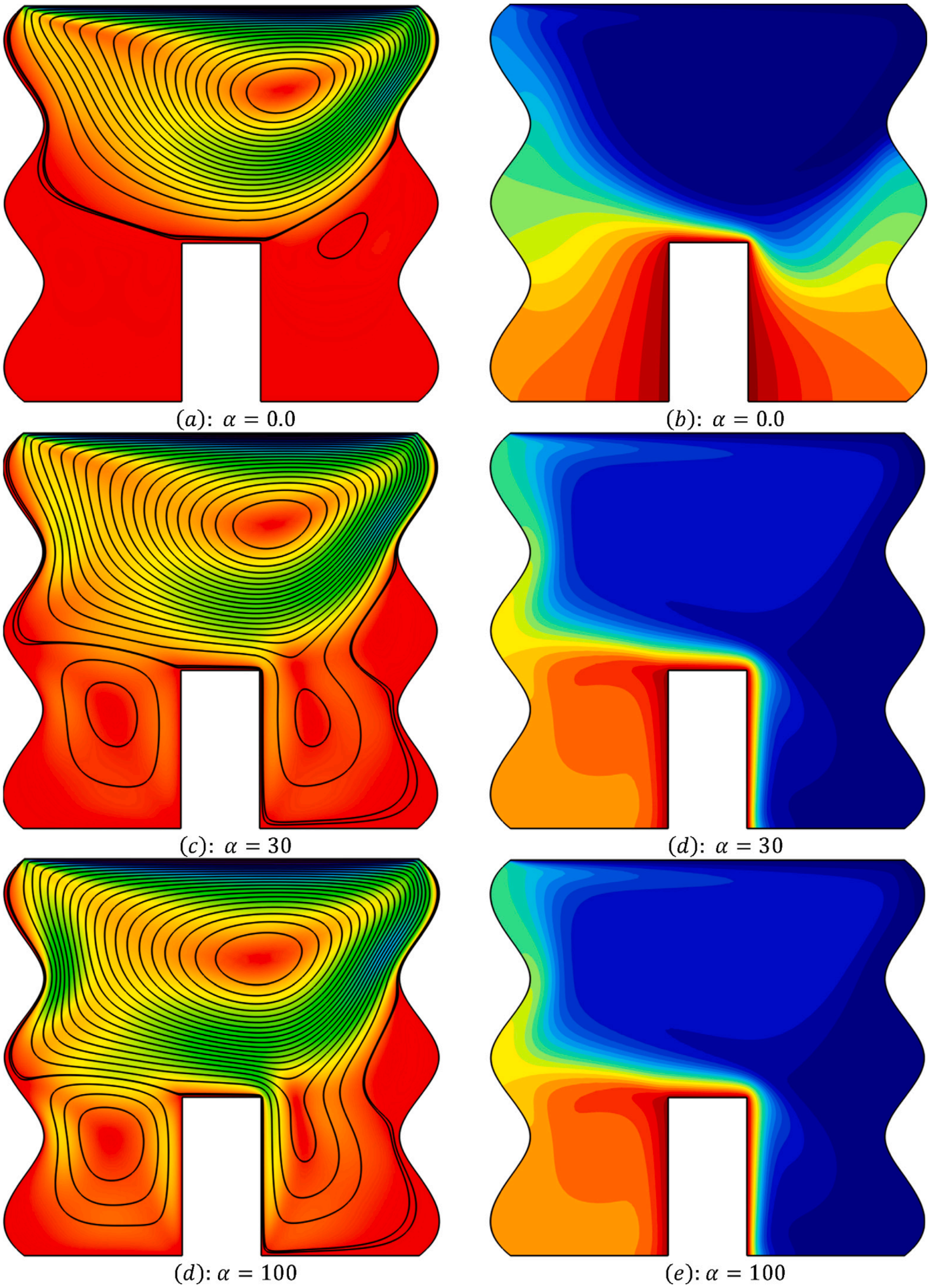

Fig. 12. Impact of mixed convection parameter on streamlines and isotherms.

Fig. 17 shows the inaccuracy for the specified model at each data point. Because the MSE values are quite low, it is clear that the ANN model that has been developed will generate very accurate results. Analysing the mean squared errors (MSEs) calculated from the data points shows that the outcomes are approaching zero. Training the multi-layer propagating network model to obtain values very near zero is clearly visible. The degree to which the built-in neural network's outputs correspond to the desired target data is a crucial metric for assessing the network's predictive power.

In addition, the correlation between the targeted and projected values can be found by regression analysis. When the regression graphs are near one, it means the results have been validated. Fig. 18 displays the results of the LMS regression analysis for training,

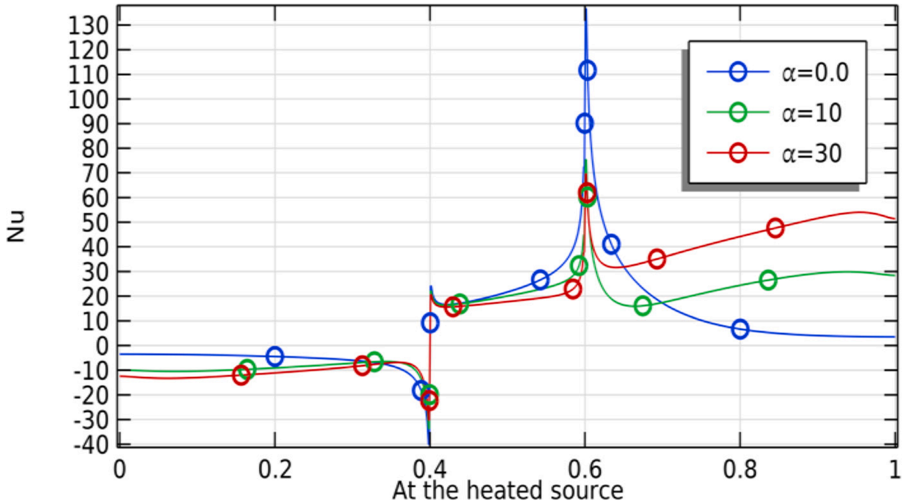

Fig. 13. Impact of mixed fraction coefficient on Nusselt number.

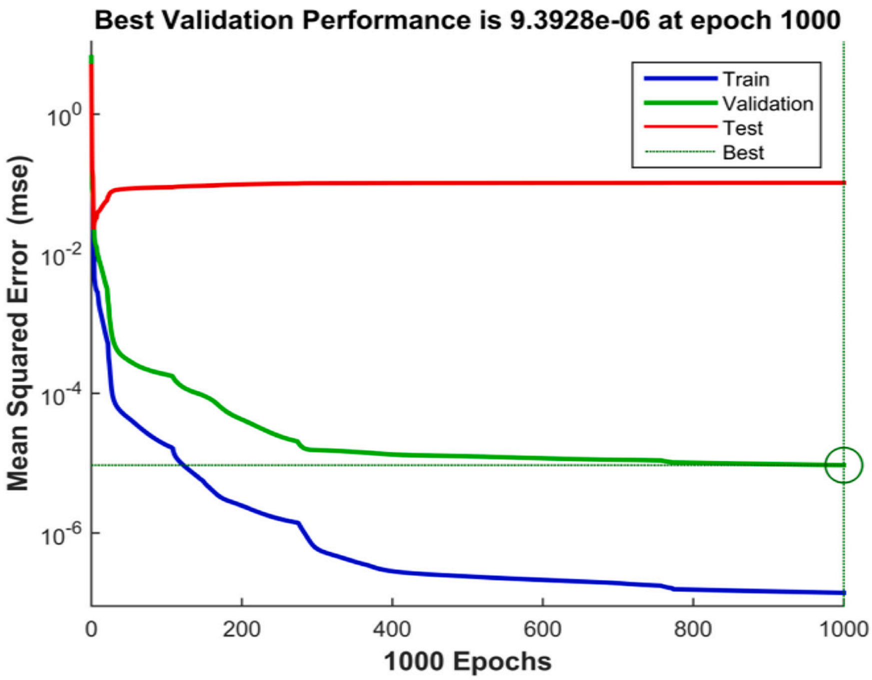

Fig. 14. MSE plot for 1000 epochs.

validation, testing, and total data. These results demonstrate a highly correlated relationship between the target and projected training outcomes, with a regression value near 1. With validation data, the regression value is 0.99999, while with testing data, it is 0.8279. Statistical analysis has shown that models with an R-squared value of 0.97573 are the most accurate at predicting the Nusselt number.

The further analysis is also done to get insight into the behaviour of flow velocity and temperature within the wavy cavity. Fig. 19(a–b) illustrates the impact of $0 \leq M \leq 20$ on velocity and temperature profile. It is observed that both profiles are showing a decrease as the magnetic impact increases due to the resistance of Lorentz force. By facilitating more effective heat transmission within the fluid and lowering the temperature gradient, this higher thermal conductivity promotes fluid motion, as seen in Fig. 20(a). Fig. 20(b) shows the decrease in temperature due to the higher impact of volume fraction. Fig. 21(a–b) shows the changing behaviour of fluid velocity and temperature. Due to stratification in density, the flow has higher kinetic energy than potential energy. Thus, velocity is increasing for escalating values of Ri. Higher Richardson numbers result in lower temperatures

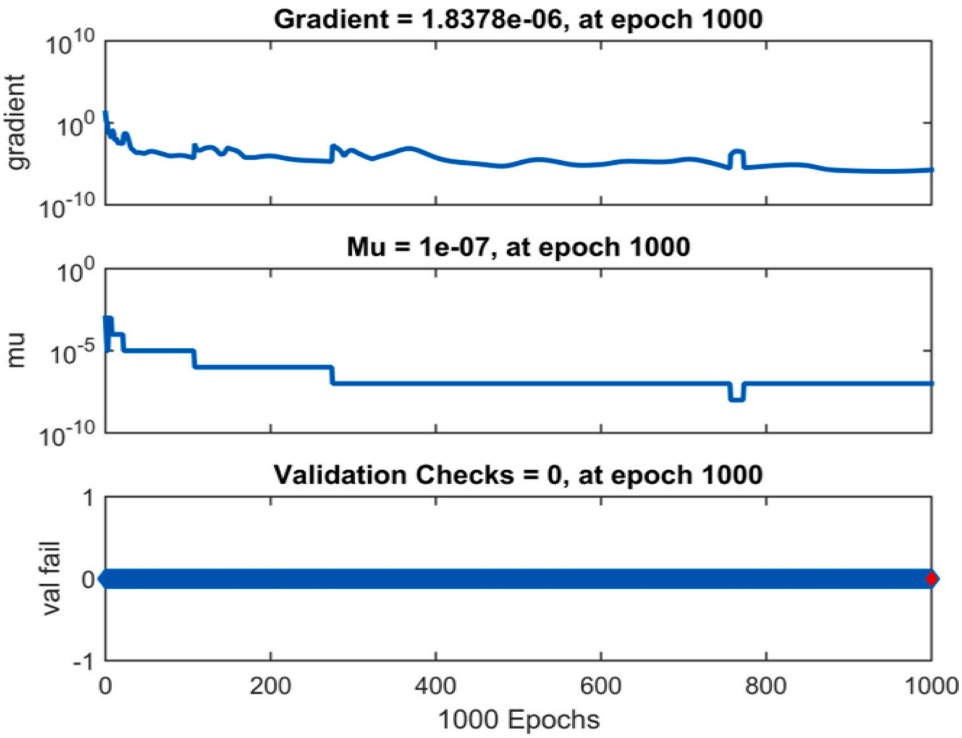

Fig. 15. Training state plot for 1000 epochs.

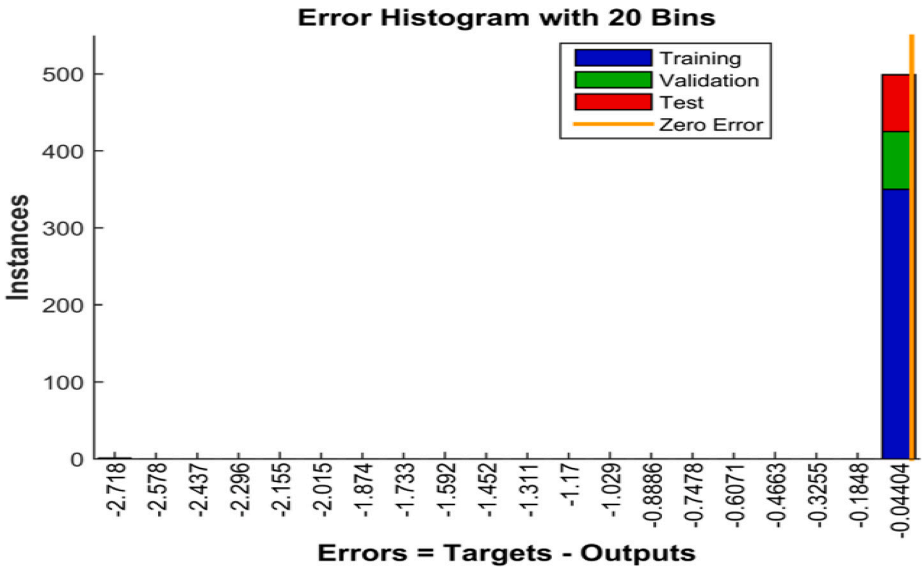

Fig. 16. Error histogram.

because more stable conditions are indicated by higher values of Ri. The vertical mixing of heat is inhibited in stable flows because shear forces predominate over buoyancy forces. Fig. 22(a) illustrates that velocity is decreasing for $50 \leq Re \leq 1000$ due to the formation of more eddies. In Fig. 22(b), Re > 100 results in lower fluid temperatures because of the greater heat transfer brought on by turbulent flows, which effectively distributes thermal energy throughout the fluid. In Fig. 23(a–b), the velocity is escalating due to the dominance of buoyant forces for higher alpha. The temperature shows an increase but gradually decreases for rising values of the nonlinear mixed convection parameter. Due to buoyancy effects, the fluid experiences larger convective currents with

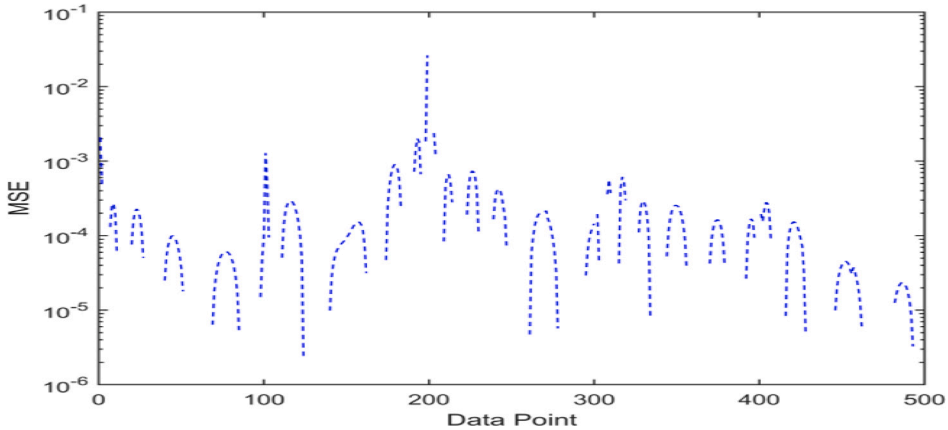

Fig. 17. Error analysis.

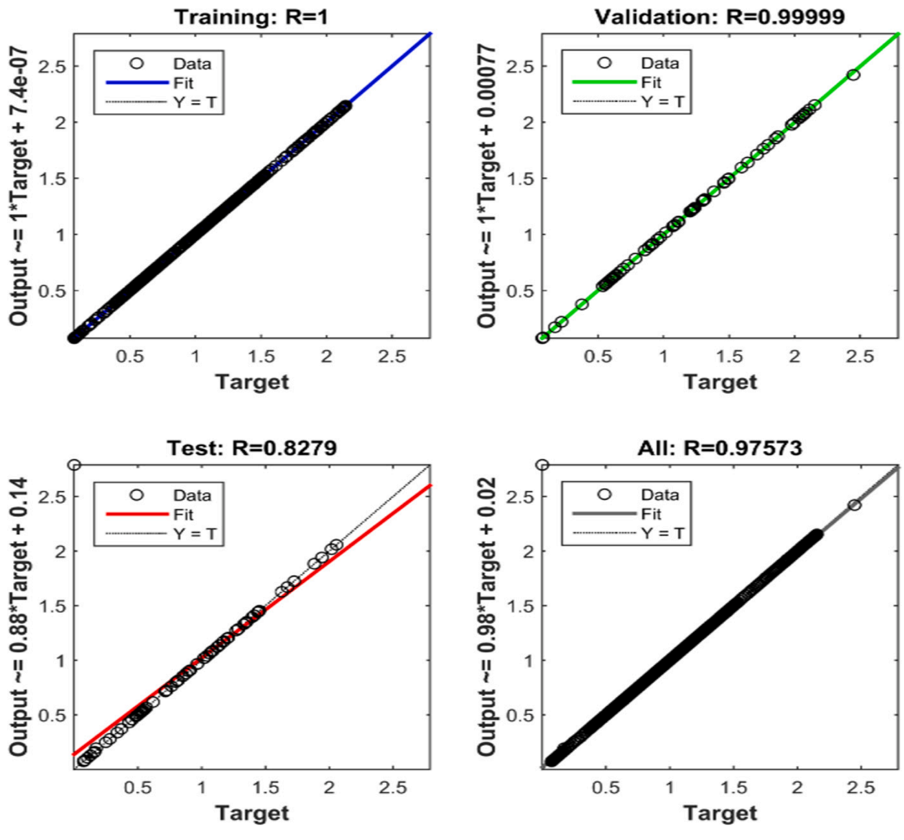

Fig. 18. Regression analysis.

higher nonlinear mixed convection. As a result of these convective currents, hot and cold fluid regions are mixed together more efficiently, which lowers the temperature differential between them overall.

6. Conclusion

The present study investigates the effects of magneto-hybrid nanofluid flow on nonlinear mixed convection characteristics within a wavy enclosure containing an enclosed heated source. A comprehensive numerical simulation has been conducted, and the influence of different parameters has been systematically analysed. The system of nonlinear PDEs is converted into a dimensionless system by using suitable transformations. These governing equations are solved by using COMSOL to get the datasets for further

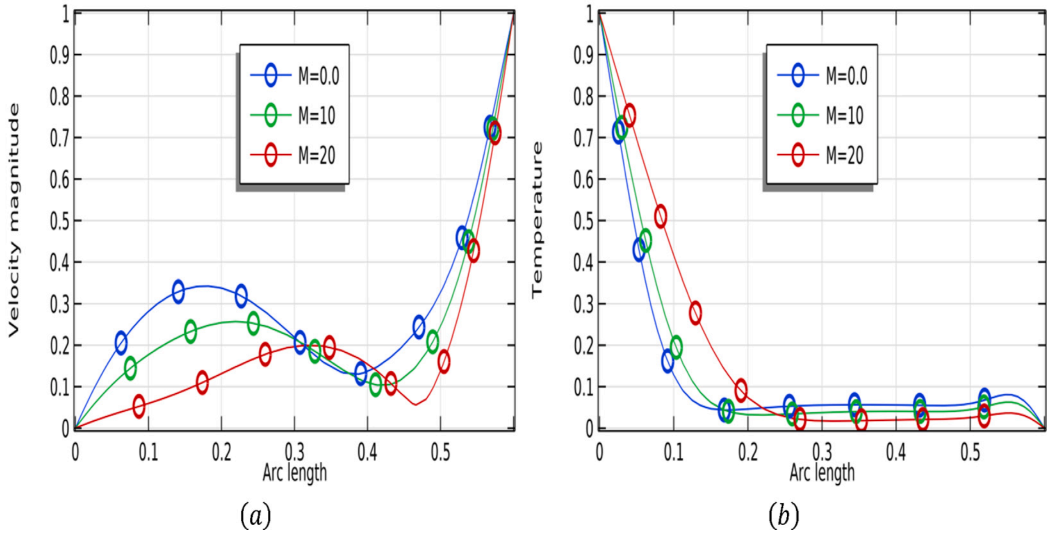

Fig. 19. Impact of magnetic parameter on velocity and temperature.

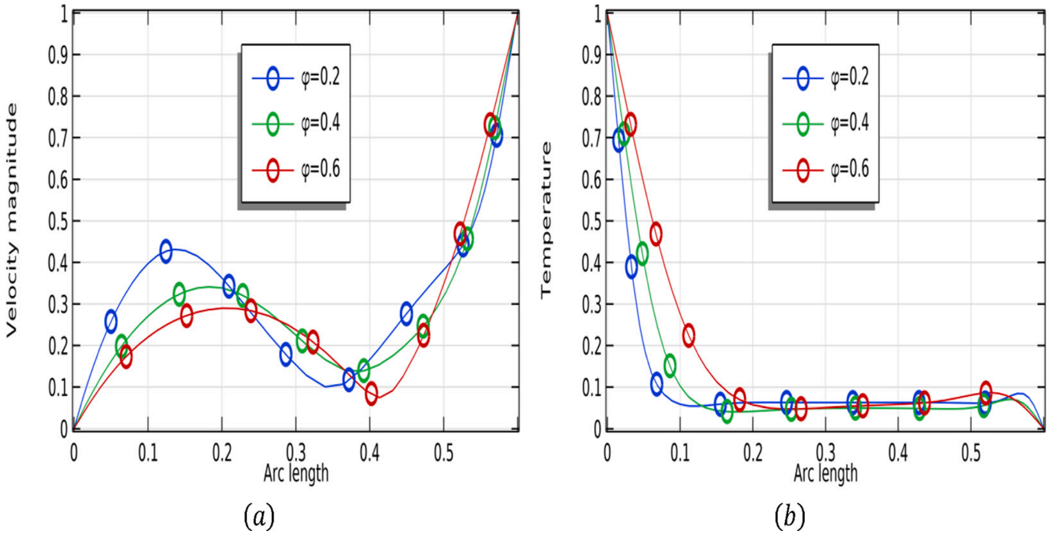

Fig. 20. Impact of volume fraction on velocity and temperature.

calculations. These datasets are divided into training, testing, and validation through Levenberg–Marquardt scheme. The proficiency of the results is obtained from MSE, regression fitness, and error histogram. The analysis give rise to following findings:

- An increase in velocity is observed for higher concentrations of hybrid nanofluids, whereas temperature decreases with the same concentration.
- Additionally, for higher Richardson numbers (Ri), the temperature exhibits a gradual decrease, while the velocity shows an escalation for the corresponding values.
- Furthermore, with increasing Reynolds number (Re) and thermal diffusivity parameter α, velocity shows an opposite behaviour for each case, while the temperature declines in both situations.
- The best MSE value obtained at 1000 epoch is $9.3928e^{-6}$. This value is very small which shows better performance of the network.
- The convergence is obtained quickly for the low values of gradient and Mu.
- In histogram plots, it is obvious that error lies with zero line and is close to −0.04404. The results are very accurate, with only a little margin of error between the projected and actual outcomes.

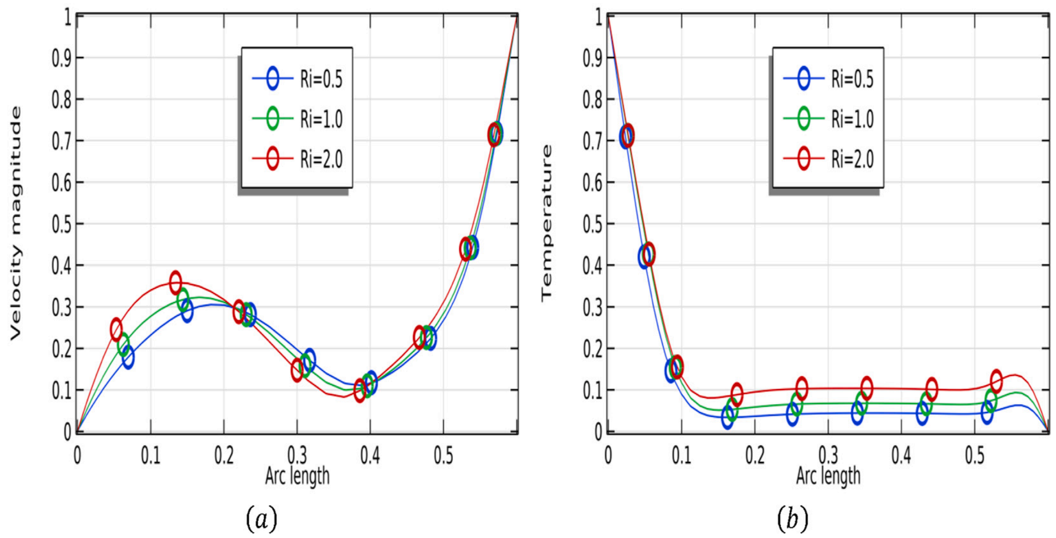

Fig. 21. Impact of Richardson parameter on velocity and temperature.

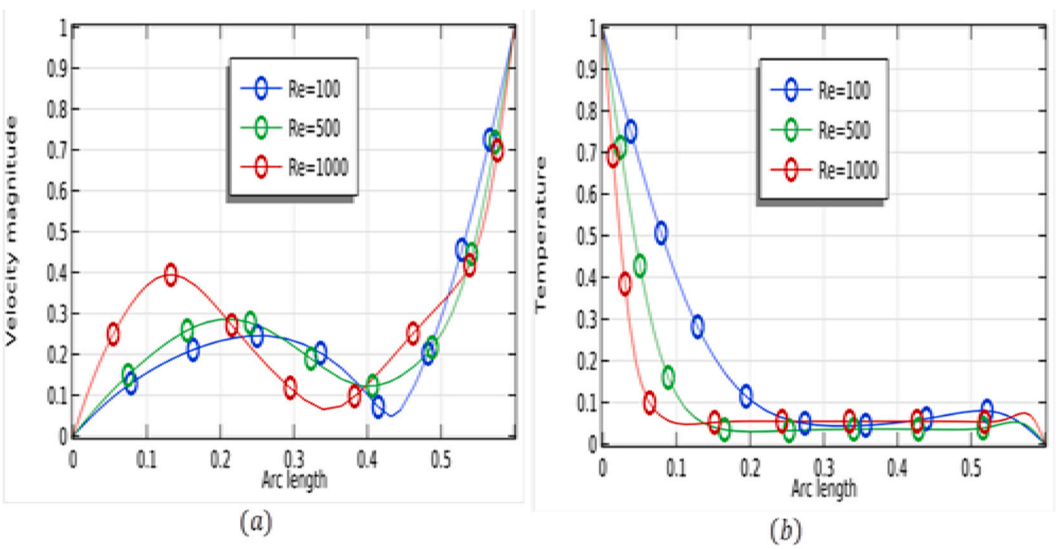

Fig. 22. Impact of Reynolds parameter on velocity and temperature.

- In regression analysis, R getting closer to 1 means, the predicted results are getting closer to original data. It is observable in above analysis. Hence, the ANN predicts better values for Nusselt number with good accuracy.
- The observations shows that LMS has provided better validation of the results in less time.
- Among the many benefits of ANN is their capacity to provide predicted values for large datasets. Across the whole range of numbers in the dataset, as well as between any two sample points, they perform exceptionally well when predicting values.

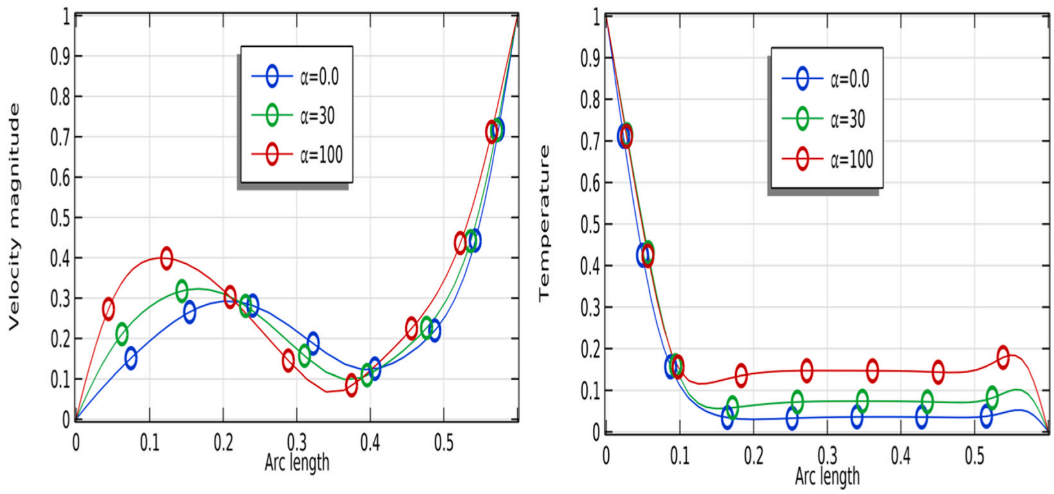

Fig. 23. Impact of nonlinear mixed convection parameter on velocity and temperature.

CRediT authorship contribution statement

Arooj Tanveer: Writing – original draft, Software, Methodology, Investigation, Conceptualization. **Sami-ul-Haq:** Writing – review & editing, Formal analysis, Conceptualization. **Muhammad Bilal Ashraf:** Writing – review & editing, Validation, Supervision. **JongSuk Ro:** Funding acquisition, Conceptualization.

Declaration of competing interest

The authors declare that they have no known competing financial interests or personal relationships that could have appeared to influence the work reported in this paper.

Acknowledgments

(1) This work was supported by the National Research Foundation of Korea(NRF) grant funded by the Korea government(MSIT) (No. NRF-2022R1A2C2004874).

(2) This work was supported by the Korea Institute of Energy Technology Evaluation and Planning(KETEP) and the Ministry of Trade, Industry & Energy(MOTIE) of the Republic of Korea (No. 20214000000280)

Data availability

Data will be made available on request.

References

[1] S. Alqaed, J. Mustafa, M. Sharifpur, Numerical investigation and optimization of natural convection and entropy generation of alumina/H2O nanofluid in a rectangular cavity in the presence of a magnetic field with artificial neural networks, Eng. Anal. Bound. Elem. 140 (2022) 507–518.
[2] D.K. Mandal, N. Biswas, N.K. Manna, D.K. Gayen, R.S. Gorla, A.J. Chamkha, Thermo-fluidic transport process in a novel M-shaped cavity packed with non-Darcian porous medium and hybrid nanofluid: Application of artificial neural network (ANN), Phys. Fluids 34 (3) (2022).
[3] P. Rana, A. Kumar, G. Gupta, Impact of different arrangements of heated elliptical body, fins and differential heater in MHD convective transport phenomena of inclined cavity utilizing hybrid nanoliquid: Artificial neutral network prediction, Int. Commun. Heat Mass Transfer 132 (2022) 105900.
[4] A. Abderrahmane, A. Mourad, S. Mohammed, G.F. Smaisim, D. Toghraie, A. Koulali, K. Guedri, O. Younis, Second law analysis of a 3D magnetic buoyancy-driven flow of hybrid nanofluid inside a wavy cubical cavity partially filled with porous layer and non-Newtonian layer, Ann. Nucl. Energy 181 (2023) 109511.
[5] A. Chattopadhyay, R. Malo, H.F. Öztop, S.K. Pandit, K.D. Goswami, Simulation of magneto mixed convective flow and thermal behavior of hybrid nanofluid in a partially heated wavy cavity, J. Magn. Magn. Mater. 575 (2023) 170713.
[6] H.R. Ashorynejad, A. Shahriari, MHD natural convection of hybrid nanofluid in an open wavy cavity, Results Phys. 9 (2018) 440–455.
[7] A.I. Alsabery, I. Hashim, A. Hajjar, M. Ghalambaz, S. Nadeem, M. Saffari Pour, Entropy generation and natural convection flow of hybrid nanofluids in a partially divided wavy cavity including solid blocks, Energies 13 (11) (2020) 2942.
[8] A.I. Alsabery, H.T. Kadhim, M.A. Ismael, I. Hashim, A.J. Chamkha, Impacts of amplitude and heat source on natural convection of hybrid nanofluids into a wavy enclosure via heatline approach, Waves Random Complex Media (2021) 1–25.

[9] Z. Raizah, A.M. Aly, N. Alsedais, M.A. Mansour, MHD mixed convection of hybrid nanofluid in a wavy porous cavity employing local thermal non-equilibrium condition, Sci. Rep. 11 (1) (2021) 17151.
[10] N. Alipour, B. Jafari, K. Hosseinzadeh, Optimization of wavy trapezoidal porous cavity containing mixture hybrid nanofluid (water/ethylene glycol Go–Al2O3) by response surface method, Sci. Rep. 13 (1) (2023) 1635.
[11] A. Mourad, A. Aissa, F. Mebarek-Oudina, W. Jamshed, W. Ahmed, H.M. Ali, A.M. Rashad, Galerkin finite element analysis of thermal aspects of Fe3O4-MWCNT/water hybrid nanofluid filled in wavy enclosure with uniform magnetic field effect, Int. Commun. Heat Mass Transfer 126 (2021) 105461.
[12] C. Revnic, T. Groşan, M. Sheremet, I. Pop, Numerical simulation of MHD natural convection flow in a wavy cavity filled by a hybrid Cu-Al 2 O 3-water nanofluid with discrete heating, Appl. Math. Mech. 41 (2020) 1345–1358.
[13] Nirmalendu Biswas, Milan K. Mondal, Dipak Kumar Mandal, Nirmal K. Manna, Rama Subba Reddy Gorla, Ali J. Chamkha, A narrative loom of hybrid nanofluid-filled wavy walled tilted porous enclosure imposing a partially active magnetic field, Int. J. Mech. Sci. 217 (2022) 107028.
[14] Dipak Kumar Mandal, Nirmalendu Biswas, Nirmal K. Manna, Rama Subba Reddy Gorla, Ali J. Chamkha, Hybrid nanofluid magnetohydrodynamic mixed convection in a novel W-shaped porous system, Internat. J. Numer. Methods Heat Fluid Flow 33 (2) (2023) 510–544.
[15] A.S. Dogonchi, Ali J. Chamkha, D.D. Ganji, A numerical investigation of magneto-hydrodynamic natural convection of Cu–water nanofluid in a wavy cavity using CVFEM, J. Therm. Anal. Calorim. 135 (4) (2019) 2599–2611.
[16] M.A. Mansour, M.A. Bakier, Magnetohydrodynamic mixed convection of TiO2–Cu/water between the double lid-driven cavity and a central heat source surrounding by a wavy tilted domain of porous medium under local thermal non-equilibrium, SN Appl. Sci. 5 (2) (2023) 51.
[17] I. Rahmoune, S. Bougoul, MHD natural convection in a cavity partially heated having a wavy wall and filled with Al2O3-water nanofluid, Algerian J. Eng. Technol. 8 (1) (2023) 84–93.
[18] X. Jiang, M. Hatami, A. Abderrahmane, O. Younis, B.M. Makhdoum, K. Guedri, Mixed convection heat transfer and entropy generation of MHD hybrid nanofluid in a cubic porous cavity with wavy wall and rotating cylinders, Appl. Therm. Eng. 226 (2023) 120302.
[19] A.K. Hussein, S.E. Ahmed, M.A. Mansour, O. Younis, L. Kolsi, Effects of radiation and heat generation on MHD mixed convection in a double lid-driven inclined wavy porous cavity filled with non-Newtonian nanofluid and including a cross-shape heaters, Waves Random Complex Media (2022) 1–28.
[20] G.H.R. Kefayati, R.R. Huilgol, Lattice Boltzmann method for simulation of mixed convection of a Bingham fluid in a lid-driven cavity, Int. J. Heat Mass Transfer 103 (2016) 725–743.